Collection SFN **7** (2007) s147–s170

Inelastic longitudinal and spherical neutron polarimetry

L.P. Regnault[1]

[1] *CEA-Grenoble, Département de Recherche Fondamentale sur la Matière Condensée, SPSMS-MDN, 17 rue des Martyrs, 38054 Grenoble Cedex 9, France*

Abstract. In this lecture we will present the general principles of the longitudinal and spherical neutron polarization analysis, with special emphasis for the inelastic-neutron-scattering case. The power of the inelastic neutron polarimetry will be illustrated on characteristic examples selected in the fields of anomalous rare-earth magnetism, classical and quantum spin magnetism and high T_c superconductivity.

1 NOTATIONS

$\mathbf{k}_0$	Incident neutron wave vector (also noted $\mathbf{k}_i$)
$\mathbf{k}_1$	Scattered neutron wave vector (also noted $\mathbf{k}_f$)
$\mathbf{Q}$	Scattering vector ($\mathbf{Q} = \mathbf{k}_0 - \mathbf{k}_1$)
Q	Modulus of $\mathbf{Q}$
E_0	Incident neutron energy (also noted E_i)
E_1	Incident neutron energy (also noted E_f)
$\hbar\omega$	Energy transfer ($\hbar\omega = E_0 - E_1$)
$\mathbf{H}_N$	Reciprocal lattice vector ($\mathbf{H}_N = (h_N, k_N, l_N)$)
$\mathbf{P}_0$	Incident polarization vector
P_0	Incident polarization absolute value
$P_{0\alpha}$	α^{th} component of incident polarization
$\mathbf{P}$	Scattered polarisation vector
P_α	α^{th} component of scattered polarization
$P_{\alpha\beta}$	Component $\alpha\beta$ of the polarization matrix
N_Q	Nuclear scattering amplitude operator for scattering vector $\mathbf{Q}$
$\mathbf{M}_Q$	Magnetic scattering amplitude operator for scattering vector $\mathbf{Q}$
$M_{Q\alpha}$	αth component of the magnetic scattering amplitude operator
$\mathbf{M}_{\perp Q}$	Magnetic interaction operator for scattering vector $\mathbf{Q}$
$M_{\perp Q\alpha}$	α^{th} component of the magnetic interaction operator
$\mathbf{k}$	Magnetic propagation vector
$\mathbf{q}$	Excitation wave vector
$S_{\alpha\beta}(\mathbf{q},\omega)$	Structure factor associated with magnetic components α and β
A^+	Adjoint of operator A
A^*	Complex conjugate of A
$\mathbf{R}_{ni}$	Atomic position vector in the nth cell, ith Bravais sublattice
T	Sample temperature
$\mathbf{H}$	Magnetic field vector
H_α	αth component of $\mathbf{H}$

2 INTRODUCTION

In this chapter we will tackle the main aspects associated with the use of polarized neutrons and neutron polarimetry in inelastic neutron scattering. Unpolarized neutron scattering is recognized to be an invaluable technique for the investigation of the lattice and spin dynamics of a great variety of materials. However, in some particular cases the structural and magnetic degrees of freedom give rise to contributions which are either superposed, or, in the most complicated cases, which strongly interfere, giving rise possibly to *hybrid modes*. In these very interesting cases, the conventional (i.e. unpolarized) neutron inelastic scattering shows its limits and a more sophisticated method must be used to solve the problem. As for the diffraction case (see previous chapters), in many studies the use of polarized neutron scattering in association with an accurate polarization analysis method is the only manner to get unambiguous pieces of information. Polarized neutron inelastic scattering is essential for measurements requiring the clean separation of magnetic and structural contributions, the independent determination of various components of dynamical magnetic excitations or fluctuations, the investigation of hybrid correlation functions coupling different (spin-lattice, orbit-lattice), or identical (spin-orbit, chiral) degrees of freedom.

3 INELASTIC NEUTRON POLARIMETRY: THEORY AND PRACTICE

The theoretical framework of the neutron-matter interaction has been developed many years ago [1,2,3,4, 5,6,7]. In this section, we will recall the main formulas essential for the understanding of the neutron polarimetry on inelastic signals. The general equations giving the polarization of the scattered beam and the inelastic differential cross section as a function of the incident polarization have been established in the early 60's by Maleyev et *al* [3,6] and Blume [7]. Denoting $\mathbf{k}_0$ and $\mathbf{k}_1$ the incident and final neutron wave vectors and $\mathbf{P}_0$ the incident neutron polarization, the neutron polarization after scattering, $\mathbf{P}$, is given by the following equation [9,10,11]:

$$\begin{aligned}\mathbf{P}(d^2\sigma/d\Omega\, d\omega) = C_p \frac{k_1}{k_0}\{&\langle N_Q N_Q^+\rangle_\omega \mathbf{P}_0 \\ &+\langle(\mathbf{P}_0\cdot\mathbf{M}_{\perp Q}^+)\mathbf{M}_{\perp Q}\rangle_\omega + \langle\mathbf{M}_{\perp Q}^+(\mathbf{P}_0\cdot\mathbf{M}_{\perp Q})\rangle_\omega \\ &-\langle\mathbf{M}_{\perp Q}\cdot\mathbf{M}_{\perp Q}^+\rangle_\omega\mathbf{P}_0 + i\,\langle\mathbf{M}_{\perp Q}\times\mathbf{M}_{\perp Q}^+\rangle_\omega \\ &+\langle N_Q^+\mathbf{M}_{\perp Q}\rangle_\omega + \langle\mathbf{M}_{\perp Q}^+ N_Q\rangle_\omega \\ &+i\,\mathbf{P}_0\times[\langle\mathbf{M}_{\perp Q}^+ N_Q\rangle_\omega - \langle N_Q^+\mathbf{M}_{\perp Q}\rangle_\omega]\}\end{aligned} \tag{3.1}$$

where $(d^2\sigma/d\Omega\, d\omega)$, the inelastic double-differential cross section, is given by:

$$\begin{aligned}d^2\sigma/d\Omega\, d\omega = C_\sigma \frac{k_1}{k_0}\{&\langle N_Q N_Q^+\rangle_\omega \\ &+\langle\mathbf{M}_{\perp Q}\cdot\mathbf{M}_{\perp Q}^+\rangle_\omega - i\,\mathbf{P}_0\cdot\langle\mathbf{M}_{\perp Q}\times\mathbf{M}_{\perp Q}^+\rangle_\omega \\ &+\mathbf{P}_0\cdot[\langle N_Q^+\mathbf{M}_{\perp Q}\rangle_\omega + \langle\mathbf{M}_{\perp Q}^+ N_Q\rangle_\omega]\}\end{aligned} \tag{3.2}$$

In Eqs.(3.1) and (3.2), C_p and C_σ are two scaling factors, $\mathbf{Q} = \mathbf{k}_0 - \mathbf{k}_1$ is the scattering vector (alias neutron momentum transfer),
$N_Q = N^{1/2}\sum_j b_j e^{i\mathbf{Q}\cdot\mathbf{R}_j}$ is the (complex) scalar nuclear scattering amplitude operator, where $\mathbf{R}_j$ and b_j are respectively the position vector and the scattering length of the j^{th} nucleus, and N is the total number of nuclei in the system. The angular brackets denote the Gibbs average as well as the average

on the spin states of the incident beam. The (complex) vectorial magnetic-interaction operator is defined by the relation:

$$\mathbf{M}_{\perp Q} = r_0 N^{1/2} \sum_j \left[\mathbf{M}_j - (\mathbf{Q}\cdot\mathbf{M}_j)\cdot\mathbf{Q}/Q^2\right] e^{i\mathbf{Q}\cdot\mathbf{R}_j},$$

where $r_0 \approx 0.54\times10^{-12}$ cm and $\mathbf{M}_j = \left[\mathbf{s}_j - \frac{i}{\hbar}(\mathbf{Q}\times\mathbf{p}_j)/Q^2\right]$ depends on both the electron spin ($\mathbf{s}_j$) and momentum ($\mathbf{p}_j$) [12,13,14]. The latter term in particular will allow to probe the orbital degrees of freedom. As it is well known, only the components of $\mathbf{M_Q}$ perpendicular to the scattering vector $\mathbf{Q}$ contribute to the magnetic scattering process. Eqs.(3.1) and (3.2) contains several terms. $\langle N_Q N_Q^+\rangle_\omega$ corresponds to the purely nuclear correlation functions and does not change the initial polarization. The two terms $\langle(\mathbf{P}_0\cdot\mathbf{M}_{\perp Q}^+)\mathbf{M}_{\perp Q}\rangle_\omega + \langle\mathbf{M}_{\perp Q}^+(\mathbf{P}_0\cdot\mathbf{M}_{\perp Q})\rangle_\omega - \langle\mathbf{M}_{\perp Q}\cdot\mathbf{M}_{\perp Q}^+\rangle_\omega\mathbf{P}_0$ and $\langle\mathbf{M}_{\perp Q}\cdot\mathbf{M}_{\perp Q}^+\rangle_\omega$ correspond to the non-chiral, purely magnetic correlation functions. One can easily verify that they produce a rotation of 180° of the incident polarization vector around the magnetic interaction vector $\mathbf{M_Q}$. The cross-product $i\langle\mathbf{M}_{\perp Q}\times\mathbf{M}_{\perp Q}^+\rangle_\omega$, the so-called chiral term, is associated with antisymmetric correlation functions. Finally, the terms $\langle N_Q^+\mathbf{M}_{\perp Q}\rangle_\omega + \langle\mathbf{M}_{\perp Q}^+ N_Q\rangle_\omega$ and $i(\langle\mathbf{M}_{\perp Q}^+ N_Q\rangle_\omega - \langle N_Q^+\mathbf{M}_{\perp Q}\rangle_\omega)$, the so-called nuclear-magnetic interference (NMI) terms, are associated with cross correlation functions respectively symmetric and antisymmetric, mixing the nuclear and various magnetic components. If strong enough, the latter may induce a rotation of the polarization away from $\pm\mathbf{P}_0$, thus giving rise to off-diagonal components of the polarization matrix. Following the custom adopted in inelastic neutron scattering, the various vectorial components (x, y and z) will be labeled with respect to $\mathbf{Q}$, using the basic frame of reference defined in Figure 1.

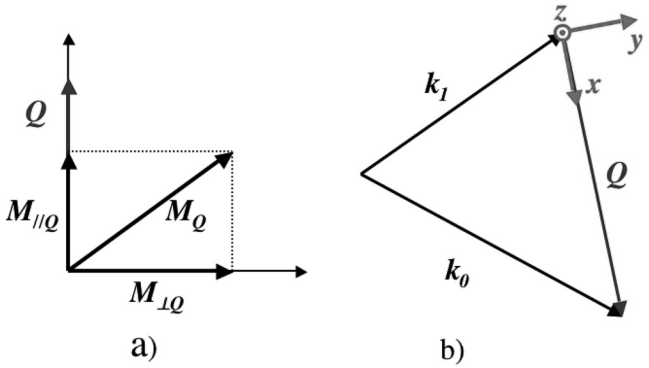

Figure 1. Geometric details of the magnetic scattering. a), the neuron selection rule: only components of $\mathbf{M_Q}$ perpendicular to $\mathbf{Q}$ contribute to the magnetic-scattering process; b), the basic frame of reference for polarization analysis: the coordinates are defined with respect to $\mathbf{Q} = \mathbf{k}_0 - \mathbf{k}_1$.

In Eqs.(3.1) and (3.2), the quantity $\langle A_Q B_Q^+\rangle_\omega$ (alias Van Hove's function [15]) is nothing else than the Fourier transform of the space and time-dependent correlation function $\langle A(\mathbf{R}_n,t)B^+(\mathbf{0},0)\rangle$:

$$\langle A_Q B_Q^+\rangle_\omega = \frac{1}{2\pi}\int_{-\infty}^{+\infty} dt\, e^{i\omega t}\sum_n \langle A(\mathbf{R}_n,t)B^+(\mathbf{0},0)e^{i\mathbf{Q}\cdot\mathbf{R}_n}\rangle \tag{3.3}$$

In some particular cases, it will be convenient to make use of the generalized susceptibilities, defined by the following relation:

$$\langle A,B\rangle_\omega = i\int_0^{+\infty} dt\, e^{i\omega t}\,\langle[A(t),B(0)]\rangle = \langle A,B\rangle'_\omega + i\,\langle A,B\rangle''_\omega \tag{3.4}$$

where$\langle A,B\rangle'_\omega$ is the dispersive part and $\langle A,B\rangle''_\omega$ the absorptive part. In the most general case, the quantity $\langle A,B\rangle''_\omega$ may be complex. From the fluctuation-dissipation theorem, one can easily establish the following general relation between $\langle AB\rangle_\omega$ and $\langle A,B\rangle''_\omega$:

$$\langle AB\rangle_\omega = \frac{1}{\pi\left(1-e^{-\hbar\omega/k_BT}\right)}\langle A,B\rangle''_\omega \tag{3.5}$$

The formulas applying to the inelastic case can be recovered from the simple replacement $\frac{k_1}{k_0}\frac{1}{\pi(1-e^{-\hbar\omega/k_BT})}$ $\langle A,B\rangle''_\omega \rightarrow \langle A\rangle\langle B\rangle$, where $\langle\rangle$ denotes the thermal average. One can easily show that the various components of the polarization matrix depend on the following nine quantities:

$$\begin{aligned}
N &= \langle N_Q N_Q^+\rangle_\omega \\
M_{yy} &= \langle M_{Qy} M_{Qy}^+\rangle_\omega \\
M_{zz} &= \langle M_{Qz} M_{Qz}^+\rangle_\omega \\
M_{ch} &= i(\langle M_{Qy} M_{Qz}^+\rangle_\omega - \langle M_{Qz} M_{Qy}^+\rangle_\omega) \\
M_{yz} &= \langle M_{Qy} M_{Qz}^+\rangle_\omega + \langle M_{Qz} M_{Qy}^+\rangle_\omega \\
R_y &= \langle N_Q M_{Qy}^+\rangle_\omega + \langle N_Q^+ M_{Qy}\rangle_\omega \\
I_y &= i(\langle N_Q M_{Qy}^+\rangle_\omega - \langle N_Q^+ M_{Qy}\rangle_\omega) \\
R_z &= \langle N_Q M_{Qz}^+\rangle_\omega + \langle N_Q^+ M_{Qz}\rangle_\omega \\
I_z &= i(\langle N_Q M_{Qz}^+\rangle_\omega - \langle N_Q^+ M_{Qz}\rangle_\omega)
\end{aligned}$$

which are, in the most general case, the nine unknown parameters of the problem. Strictly speaking, factors depending on the cross product $\mathbf{k}_0 \times \mathbf{k}_1$ appears both in the expressions of the cross section and the polarization when the relativistic [16] and spin-orbit [17] corrections are taken into account. Interestingly, such terms introduce some *handedness* in the scattering process and a right-left asymmetry may be seen in the measurements. However, these terms contain the prefactor m_e/m_n, ratio of the electron mass to the neutron mass. Obviously, such terms are expected to be about three orders of magnitude smaller than the conventional inelastic terms. They will be completely neglected in the following.

The inelastic cross section can be rewritten according to the linear form of $\mathbf{P}_0$ [11]:

$$\frac{d^2\sigma}{d\Omega}d\omega = \sigma(\mathbf{Q},\omega) = \sigma_0(\mathbf{Q},\omega) + \mathbf{P}_0\sum_0(\mathbf{Q},\omega) \tag{3.6}$$

The expression for the polarization has a similar form:

$$\mathbf{P}\sigma(\mathbf{Q},\omega) = T(\mathbf{Q},\omega)\mathbf{P}_0 + \sum_1(\mathbf{Q},\omega) \tag{3.7}$$

σ_0, $\mathbf{\Sigma}_0$ and $\mathbf{\Sigma}_1$ can be easily deduced from Eqs.(3.1) and (3.2). In Eq.(3.7), T is a second-rank tensor acting on the vector $\mathbf{P}_0$ according to the rule: $T\mathbf{P}_0 = T_{\alpha\beta}P_{0\beta}$. In the most general case, T may have a symmetric and an antisymmetric part: $T_{\alpha\beta} = T^S_{\alpha\beta} + \sum_\gamma \epsilon_{\alpha\beta\gamma}A_\gamma$, where $\epsilon_{\alpha\beta\gamma}$ is a third-rank unit pseudo-tensor and $\mathbf{A}$ is an axial vector. Eq.(3.7) can be rewritten as:

$$\mathbf{P}\sigma(\mathbf{Q},\omega) = T^S(\mathbf{Q},\omega)\mathbf{P}_0 + \mathbf{A}\times\mathbf{P}_0 + \mathbf{\Sigma}_1(\mathbf{Q},\omega) \tag{3.8}$$

Eq.(3.8) reveals the following very important fact: **the transverse components of the polarization can only arise from the antisymmetric part and result necessarily from the existence of an axial vector in the problem**.

Up to now, we have implicitly assumed that the nuclei were lacking in spin. The complete derivation taking into account the effects of the nuclear spin has been undertaken by Blume a long time ago [8]. Without entering into the details, it has been shown that the expressions of the polarization and the cross section for the nuclear subsystem were quite similar to Eqs.(3.1) and (3.2), the only difference being that, this time, the three components of the nuclear spin I_α ($\alpha = x, y, z$) play a role. In the following, we will consider only phenomena occuring at temperatures located above the Kelvin scale. At such temperatures, the nuclear spins can be considered to a good approximation as completely uncorrelated (meaning that $\langle I_\alpha \rangle \approx 0$ and $\langle I_\alpha I_\beta \rangle \approx \frac{1}{3} I(I+1)\delta_{\alpha\beta}$), giving rise to the two following additional terms in the right members of Eq.(3.1) and Eq.(3.2), $\frac{k_1}{k_0}[\langle(\mathbf{P}_0 \cdot \mathbf{I}_Q^+)\mathbf{I}_Q\rangle_\omega + \langle \mathbf{I}_Q^+(\mathbf{P}_0 \cdot \mathbf{I}_Q)\rangle_\omega - \langle \mathbf{I}_Q \cdot \mathbf{I}_Q^+\rangle_\omega \mathbf{P}_0]$ and $\frac{k_1}{k_0}\langle \mathbf{I}_Q \cdot \mathbf{I}_Q^+\rangle_\omega$, respectively. As it can be easily checked from the above equations, the additional polarization due to the incoherent nuclear-spin scattering is independent on the incident polarization direction, while the corresponding cross section is a δ-function of energy ($\propto I(I+1)\delta(\omega)$), associated with a purely elastic process.

3.1 Longitudinal neutron polarimetry

Theory

The longitudinal polarization analysis (LPA) method allow to recover P_L, the projection of the final polarization $\mathbf{P}$ onto the incident polarization $\mathbf{P}_0$. In the very realistic case for which the antisymmetric NMI terms can be neglected, the expressions (3.1) and (3.2) simplify:

$$\begin{aligned}\mathbf{P}\left(\frac{d^2\sigma}{d\Omega\, d\omega}\right) = C_p\, \frac{k_1}{k_0}[&\langle N_Q N_Q^+\rangle_\omega \mathbf{P}_0 \\ &+\langle(\mathbf{P}_0 \cdot \mathbf{M}_{\perp Q}^+)\mathbf{M}_{\perp Q}\rangle_\omega + \langle \mathbf{M}_{\perp Q}^+(\mathbf{P}_0 \cdot \mathbf{M}_{\perp Q})\rangle_\omega \\ &-\langle \mathbf{M}_{\perp Q} \cdot \mathbf{M}_{\perp Q}^+\rangle_\omega \mathbf{P}_0 + i\,\langle \mathbf{M}_{\perp Q} \times \mathbf{M}_{\perp Q}^+\rangle_\omega \\ &+\langle N_Q^+ \mathbf{M}_{\perp Q}\rangle_\omega + \langle \mathbf{M}_{\perp Q}^+ N_Q\rangle_\omega] \end{aligned} \tag{3.9}$$

$$\begin{aligned}\frac{d^2\sigma}{d\Omega\, d\omega} = C_\sigma\, \frac{k_1}{k_0}[&\langle N_Q N_Q^+\rangle_\omega \\ &+\langle \mathbf{M}_{\perp Q} \cdot \mathbf{M}_{\perp Q}^+\rangle_\omega - i\,\mathbf{P}_0 \cdot \langle \mathbf{M}_{\perp Q} \times \mathbf{M}_{\perp Q}^+\rangle_\omega \\ &+\mathbf{P}_0 \cdot [\langle N_Q^+ \mathbf{M}_{\perp Q}\rangle_\omega + \langle \mathbf{M}_{\perp Q}^+ N_Q\rangle_\omega] \end{aligned} \tag{3.10}$$

the longitudinal component of the polarization being given by the relation: $P_L = \mathbf{P} \cdot \mathbf{P}_0 / P_0$. In addition to the symmetric NMI and chiral terms, which could create some polarization, Eq.(3.9) contains terms proportional to $\mathbf{P}_0$ (which do not change the incident polarization) and terms proportional to $-\mathbf{P}_0$ (which reverse completely the incident polarization). Following the usual terminology, the former will be called *non spin-flip* (NSF) terms and the latter *spin-flip* (SF) terms. Neglecting at first approximation the symmetric NMI and chiral terms, after some trivial algebra one can deduce the expressions of NSF and SF cross-sections in the different cases where $\mathbf{P}_0$ is parallel to $\mathbf{x}$, $\mathbf{y}$ and $\mathbf{z}$:

$$\begin{aligned}
&\sigma_x^{NSF}(\mathbf{Q},\omega) \propto N \\
&\sigma_x^{SF}(\mathbf{Q},\omega) \propto M_{yy} + M_{zz} \\
&\sigma_y^{NSF}(\mathbf{Q},\omega) \propto N + M_{yy} \\
&\sigma_y^{SF}(\mathbf{Q},\omega) \propto M_{zz} \\
&\sigma_z^{NSF}(\mathbf{Q},\omega) \propto N + M_{zz} \\
&\sigma_z^{SF}(\mathbf{Q},\omega) \propto M_{yy}
\end{aligned}$$

The various longitudinal components of the polarization in absence of chiral term, are deduced from the NSF and SF cross sections according to the simple relation:

$$P_{\alpha\alpha} \approx \frac{\sigma_\alpha^{NSF} - \sigma_\alpha^{SF}}{\sigma_\alpha^{NSF} + \sigma_\alpha^{SF}} P_0 \tag{3.11}$$

In the above expressions, we have again omitted the terms arising from the nuclear spins. However, from the previous discussion, it is easy to verify that the SF incoherent nuclear-spin contribution is two times larger than the NSF one [13-18], whatever the direction of $\mathbf{P}_0$ with respect to $\mathbf{Q}$ is.

As one can see, the coherent nuclear part (e.g., phonons or more complex lattice fluctuations) is always NSF. The magnetic contributions due to the unpaired electrons can be either SF or NSF, depending on the relative orientation of $\mathbf{P}_0$ with respect to $\mathbf{Q}$. The NSF and SF contributions corresponding to some typical scattering processes are summarized in Table 1. The most interesting situation is realized when $\mathbf{P}_0 // \mathbf{Q}$, because in that case the magnetic contributions are purely SF and the structural ones purely NSF. In other words, there is a complete separation of nuclear and electronic contributions. Thus, the longitudinal polarimetry offers a very elegant way to determine independently the magnetic and structural contributions, by measuring the SF and NSF cross sections in the configuration $\mathbf{P}_0 // \mathbf{Q}$.

Table 1. Proportion of NSF and SF contribution for some typical scattering process.

Type de diffusion	*NSF*	*SF*
Lattice excitations	1	0
Electron magnetic excitations	0–1/2	1–1/2
Nuclear spin incoherent	1/3	2/3
Nuclear isotopic incoherent	1	0

A simple rule allowing us to determine if a magnetic contribution is SF or NSF is the following:

1. The magnetic components parallel to $\mathbf{P}_0$ are always NSF,
2. The magnetic components perpendicular to $\mathbf{P}_0$ are always SF.

By measuring the SF or NSF cross sections (indeed the result should be the same) for the three orientations of the incident polarization, $\mathbf{P}_0 \parallel \mathbf{x}$, $\mathbf{P}_0 \parallel \mathbf{y}$ and $\mathbf{P}_0 \parallel \mathbf{z}$, it is even possible to have access independently to the different magnetic components of the electron system. This method, known in the literature as the vertical field-horizontal field (alias VH-VF) method, can even be used on polycristalline or powdered samples (see chapter 5). If the NMI and chiral terms can be neglected, the magnetic components along $\mathbf{y}$ and $\mathbf{z}$ can be determined respectively from the differences $\sigma_x^{SF} - \sigma_y^{SF}$ and $\sigma_x^{SF} - \sigma_z^{SF}$, or, quite equivalently, $\sigma_y^{NSF} - \sigma_x^{NSF}$ and $\sigma_z^{NSF} - \sigma_x^{NSF}$ [19]. This method presents the big advantage of eliminating the background and the nuclear contributions from the problem (owing to the fact that both are independent of the polarization direction with respect to the scattering vector $\mathbf{Q}$), but has the big disadvantage of being much time-consuming.

In the quite general case for which the symmetric NMI and antisymmetric chiral terms cannot be neglected, the four different differential cross sections, $\sigma^{++} = (d^2\sigma/d\Omega\, d\omega)^{++}$, $\sigma^{--} = (d^2\sigma/d\Omega\, d\omega)^{--}$, $\sigma^{+-} = (d^2\sigma/d\Omega\, d\omega)^{+-}$ and $\sigma^{-+} = (d^2\sigma/d\Omega\, d\omega)^{-+}$ for an initial polarization applied respectively along $\mathbf{x}$, $\mathbf{y}$ or $\mathbf{z}$, deduced from Eq.(3.10), are given by the following expressions:

$$\begin{aligned}
\sigma_x^{++} &\propto N \\
\sigma_x^{--} &\propto N \\
\sigma_x^{+-} &\propto M_{yy} + M_{zz} - M_{ch} \\
\sigma_x^{-+} &\propto M_{yy} + M_{zz} + M_{ch}
\end{aligned}$$

$$
\begin{aligned}
\sigma_y^{++} &\propto N + M_{yy} + R_y \\
\sigma_y^{--} &\propto N + M_{yy} - R_y \\
\sigma_y^{+-} &\propto M_{zz} \\
\sigma_y^{-+} &\propto M_{zz} \\
\sigma_z^{++} &\propto N + M_{zz} + R_z \\
\sigma_z^{--} &\propto N + M_{zz} - R_z \\
\sigma_z^{+-} &\propto M_{yy} \\
\sigma_z^{-+} &\propto M_{yy}
\end{aligned}
$$

in which M_{ch} is the chiral term and R_α ($\alpha = y, z$) are the symmetric NMI terms coupling the nuclear components and the magnetic ones in the direction α. For a beam initially unpolarized (e.g. for a graphite-Heusler configuration), the various cross sections for a polarization analyzed along the $\mathbf{x}$, $\mathbf{y}$ et $\mathbf{z}$ are given by the relations:

$$
\begin{aligned}
\sigma_x^{0+} &\propto N + M_{yy} + M_{zz} + M_{ch} \\
\sigma_x^{0-} &\propto N + M_{yy} + M_{zz} - M_{ch} \\
\sigma_y^{0+} &\propto N + M_{yy} + M_{zz} + R_y \\
\sigma_y^{0-} &\propto N + M_{yy} + M_{zz} - R_y \\
\sigma_z^{0+} &\propto N + M_{yy} + M_{zz} + R_z \\
\sigma_z^{0-} &\propto N + M_{yy} + M_{zz} - R_z
\end{aligned}
$$

Symmetrically, in absence of polarization analysis (e.g. for a graphite-Heusler configuration), one can define the following cross sections:

$$
\begin{aligned}
\sigma_x^{+0} &\propto N + M_{yy} + M_{zz} - M_{ch} \\
\sigma_x^{-0} &\propto N + M_{yy} + M_{zz} + M_{ch} \\
\sigma_y^{+0} &\propto N + M_{yy} + M_{zz} + R_y \\
\sigma_y^{-0} &\propto N + M_{yy} + M_{zz} - R_y \\
\sigma_z^{+0} &\propto N + M_{yy} + M_{zz} + R_z \\
\sigma_z^{-0} &\propto N + M_{yy} + M_{zz} - R_z
\end{aligned}
$$

The six structure factors N, M_{yy}, M_{zz}, M_{ch}, R_y and R_z can be determined separately from linear combinations of previous relations, according to the following set of equations:

$$
\begin{aligned}
N &\propto \sigma_x^{++} = \sigma_x^{--} \\
M_{yy} &\propto \frac{\sigma_y^{++} + \sigma_y^{--}}{2} - \frac{\sigma_x^{++} + \sigma_x^{--}}{2} = \frac{\sigma_x^{+-} + \sigma_x^{-+}}{2} - \frac{\sigma_y^{+-} + \sigma_y^{-+}}{2} \\
M_{zz} &\propto \frac{\sigma_z^{++} + \sigma_z^{--}}{2} - \frac{\sigma_x^{++} + \sigma_x^{--}}{2} = \frac{\sigma_x^{+-} + \sigma_x^{-+}}{2} - \frac{\sigma_z^{+-} + \sigma_z^{-+}}{2} \\
M_{ch} &\propto \frac{\sigma_x^{-+} - \sigma_x^{+-}}{2} = \frac{\sigma_x^{0+} - \sigma_x^{0-}}{2} = -\frac{\sigma_x^{+0} - \sigma_x^{-0}}{2}
\end{aligned}
$$

$$R_y \propto \frac{\sigma_y^{++} - \sigma_y^{--}}{2} = \frac{\sigma_y^{0+} - \sigma_y^{0-}}{2} = \frac{\sigma_y^{+0} - \sigma_y^{-0}}{2}$$
$$R_z \propto \frac{\sigma_z^{++} - \sigma_z^{--}}{2} = \frac{\sigma_z^{0+} - \sigma_z^{0-}}{2} = \frac{\sigma_z^{+0} - \sigma_z^{-0}}{2}$$

which is nothing else than a generalization of the HF-VF method. Note that the three others structure factors M_{yz}, I_y and I_z cannot be determined by LPA. They are only reachable from SNP. Alternately, M_{ch}, R_y and R_z can be determined by measuring the polarization creation respectively in the direction $\mathbf{x}$, $\mathbf{y}$ or $\mathbf{z}$, starting from an initially unpolarized beam (P_0=0):

$$P_x \approx \frac{M_{ch}}{\sigma_0} \tag{3.12}$$
$$P_y \approx \frac{R_y}{\sigma_0} \tag{3.13}$$
$$P_z \approx \frac{R_z}{\sigma_0} \tag{3.14}$$

in which $\sigma_0 = N + M_{yy} + M_{zz}$ is related to the total unpolarized structure factor. Among other, the longitudinal polarization analysis will be particularly useful for the accurate determination of the anisotropy of dynamical magnetic correlation functions. For an isotropic magnetic system, the polarization depends only on the relative direction of $\mathbf{Q}$ and $\mathbf{P}_0$:

$$\mathbf{P} \approx -\frac{\mathbf{Q}(\mathbf{Q} \cdot \mathbf{P}_0)}{Q^2} \tag{3.15}$$

This expression, established a longtime ago [1], was first checked experimentally from small-angle scattering on nickel [20]. Let come back to the the problem of the measurement of a small inelastic nuclear contribution superposed to a large inelastic magnetic one, in absence of chiral term ($M_{ch} \approx 0$). From Eq.(3.9) one can establish the following important relation between the three longitudinal (diagonal) components P_{xx}, P_{yy} and P_{zz} of the polarization matrix, and the nuclear contribution N:

$$\frac{P_{xx} + P_{yy} + P_{zz}}{P_0} \approx -1 + \frac{4N}{N + M_{yy} + M_{zz}} \tag{3.16}$$

Although more time-consuming than the simple method consisting to determine the nuclear correlation function directly from the measurement of the NSF contribution for $\mathbf{P}_0 \parallel \mathbf{x}$ (according to the relation: $N \propto \sigma_x^{NSF}(\mathbf{Q}, \omega) - Bck^{NSF}$), the measurement of $P_{xx} + P_{yy} + P_{zz}$ and the use of Eq.(3.16) offer the big advantage of canceling the effects of parasitic magnetic components coming either from nuclear or from electron spins (such, for example, the multiple scattering of a magnetic excitation and a structural Bragg reflection).

Experimental procedure

How are the longitudinal components of the polarization determined experimentally? Figure 2 shows the principle of the longitudinal polarimetry on three-axis spectrometer (TAS). The polarization selector is generally a system of Helmholtz coils allowing to set the polarization vector in any direction of the space. The different states $|+>$ or $|->$ of the neutron spin can be selected through a set of two flippers located on the incident and scattered beams.

The solution of the full problem, that is to say the determination of the six structure factors N, M_{yy}, M_{zz}, M_{ch}, R_y and R_z, can be obtained by measuring a minimal number of non spin-flip σ_α^{++} and σ_α^{--}, and spin flip σ_α^{+-} and σ_α^{-+} cross sections ($\alpha = x$, y and z) and applying the above relations. In practice, the procedure will consist to measure the four intensities I_α^{++}, I_α^{+-}, I_α^{-+} and I_α^{--} (or at least part of them) and, eventually, to perform the appropriate background corrections.

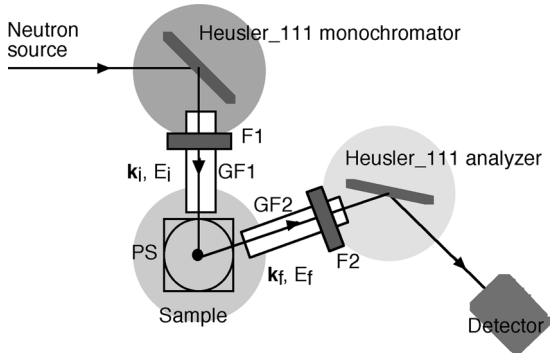

Figure 2. Principle of the longitudinal polarization analysis (LPA) on a three-axis spectrometer (GFs are guide fields; Fns are flippers; PS is the polarization selector).

3.2 Spherical neutron polarimetry

In some special cases, the NMI terms may be interesting to determine. This is the case, for example, in systems where the magnetic, lattice and charge degrees of freedom are strongly hybridized. The resulting hybrid correlation functions (spin-lattice, orbit-lattice, spin-spin, orbit-orbit, spin-orbit) may produce non-vanishing interference terms which might rotate the polarization vector slightly away from $\mathbf{P}_0$, giving rise to non-zero transverse components of polarization. As previously discussed, the observation of a sizable rotation of the polarization implies necessarily the existence of at least one axial vector in the problem. Potential candidates may be found in strongly correlated electron systems in which the spin-orbit and spin-lattice couplings are strong enough. To our best knowledge, the case of the vectorial Dzyaloshinskii-Moriya term modulated by a longitudinal lattice excitations is the only case having been investigated theoretically [9,64]. The inelastic spherical neutron polarimetry (alias SNP), in addition to the three usual longitudinal components xx, yy and zz, allows to also determine the transvserse components, xy, yx, xz, zx, yz and zy. In the next section, we will give the main relations linking the different polarization components $P_{\alpha\beta}$ to the various interference terms.

The basic relations of the inelastic SNP

In the following, it will be useful to introduce the following quantities:

$$R_\alpha = \langle M_Q^{\alpha+} N_Q \rangle_\omega + \langle M_Q^\alpha N_Q^+ \rangle_\omega \tag{3.17}$$

previously defined, characterizing the symmetric part of the INMI terms involving the magnetic components along α,

$$I_\alpha = i\,[\langle M_Q^{\alpha+} N_Q \rangle_\omega - \langle M_Q^\alpha N_Q^+ \rangle_\omega] \tag{3.18}$$

characterizing the antisymmetric part of INMI terms, and,

$$\sigma_0 = \langle N_Q N_Q^+ \rangle_\omega + \langle M_Q^y M_Q^{y+} \rangle_\omega + \langle M_Q^z M_Q^{z+} \rangle_\omega \tag{3.19}$$

which is nothing else than the total unpolarized cross section, neglecting the chiral and NMI terms, both expected to be much smaller than the usual magnetic contributions. As for the chiral term $M_{ch} = i(\langle M_Q^y M_Q^{z+} \rangle_\omega - \langle M_Q^z M_Q^{y+} \rangle_\omega)$, the real parts of NMI terms may conduce to polarize an initially unpolarized incident beam. The various components of the resulting polarization are given by the following relation:

$$P_x \approx \frac{M_{ch}}{\sigma_0} \tag{3.20}$$

$$P_y \approx \frac{R_y}{\sigma_0} \tag{3.21}$$

$$P_z \approx \frac{R_z}{\sigma_0} \tag{3.22}$$

Thus, in principle the measurements by LPA of the three components of the polarization vector after scattering should allow us to determine the chiral and the *symmetric* INMI terms. However, the determination of the antisymmetric INMI terms will necessarily require the measurement of a minimal number of transverse components by SNP. From the general equations, assuming the *inelastic* chiral and NMI terms small, it is easy to derive the following relations giving the transverse components xy, yx, xz, zx, yz, and zy (at first order):

$$P_{xy} \approx \frac{R_y}{\sigma_0} - \frac{I_z}{\sigma_0} P_0 \tag{3.23}$$

$$P_{yx} \approx \frac{M_{ch}}{\sigma_0} + \frac{I_z}{\sigma_0} P_0 \tag{3.24}$$

$$P_{xz} \approx \frac{R_z}{\sigma_0} + \frac{I_y}{\sigma_0} P_0 \tag{3.25}$$

$$P_{zx} \approx \frac{M_{ch}}{\sigma_0} - \frac{I_y}{\sigma_0} P_0 \tag{3.26}$$

$$P_{yz} \approx \frac{R_z}{\sigma_0} + \frac{M_{yz}}{\sigma_0} P_0 \tag{3.27}$$

$$P_{zy} \approx \frac{R_y}{\sigma_0} + \frac{M_{yz}}{\sigma_0} P_0 \tag{3.28}$$

where the symmetric term $M_{yz} = \langle M_Q^y M_Q^{z+} \rangle_\omega + \langle M_Q^z M_Q^{y+} \rangle_\omega$ involves correlation functions coupling magnetic components along $\mathbf{y}$ and $\mathbf{z}$, as does the antisymmetric chiral term. It is worthwhile to note that, in the most general case, the polarization matrix $P_{\alpha\beta}$ ($\alpha, \beta = x, y, z$) is not symmetric. The different structure factors can be determined *separately* from appropriate symmetric or antisymmetric combinations of transverse components measured at incident polarization $\pm\mathbf{P}_0$, according to the following relations:

$$M_{ch} \approx \frac{P_{yx} + P_{\bar{y}x}}{2}\sigma_0 \approx \frac{P_{zx} + P_{\bar{z}x}}{2}\sigma_0 \tag{3.29}$$

$$M_{yz} \approx \frac{P_{yz} - P_{\bar{y}z}}{2P_0}\sigma_0 \approx \frac{P_{zy} - P_{\bar{z}y}}{2P_0}\sigma_0 \tag{3.30}$$

$$R_y \approx \frac{P_{xy} + P_{\bar{x}y}}{2}\sigma_0 \approx \frac{P_{zy} + P_{\bar{z}y}}{2}\sigma_0 \tag{3.31}$$

$$I_y \approx \frac{P_{xz} - P_{\bar{x}z}}{2P_0}\sigma_0 \approx -\frac{P_{zx} - P_{\bar{z}x}}{2P_0}\sigma_0 \tag{3.32}$$

$$R_z \approx \frac{P_{xz} + P_{\bar{x}z}}{2}\sigma_0 \approx \frac{P_{yz} + P_{\bar{y}z}}{2}\sigma_0 \tag{3.33}$$

$$I_z \approx \frac{P_{xy} - P_{\bar{x}y}}{2P_0}\sigma_0 \approx -\frac{P_{yx} - P_{\bar{y}x}}{2P_0}\sigma_0 \tag{3.34}$$

Note that the procedure for the determination of N, M_{yy}, and M_{zz} from SNP is exactly the same as from LPA. For a purely magnetic signal (i.e. neglecting all terms involving the nuclear operator), one can deduce the following relations for the longitudinal and transverse components:

$$P_{xx} \approx -\frac{\sigma_M P_0 - M_{ch}}{\sigma_M - M_{ch} P_0} \tag{3.35}$$

$$P_{yy} \approx -P_{zz} \approx \frac{M_{yy} - M_{zz}}{\sigma_M} P_0 \tag{3.36}$$

$$P_{xy} \approx P_{xz} \approx 0 \tag{3.37}$$

$$P_{yx} \approx P_{zx} \approx \frac{M_{ch}}{\sigma_M} \tag{3.38}$$

$$P_{yz} \approx P_{zy} \approx \frac{M_{yz}}{\sigma_M} P_0 \tag{3.39}$$

in which $\sigma_M = M_{yy} + M_{zz}$ is the total magnetic structure factor. Thus, off-diagonal components $P_{yx} \approx P_{zx}$ and $P_{yz} \approx P_{zy}$ are expected in case of finite $< yz >$ cross correlation functions (indeed those giving rise to the M_{ch} and M_{yz} terms).

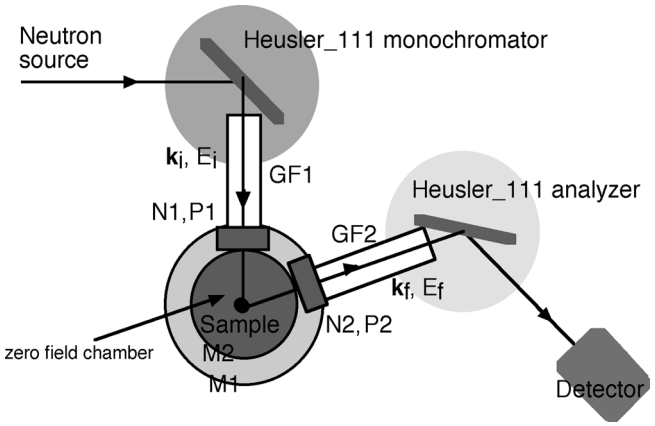

Figure 3. Principle of the spherical neutron polarimetry (SNP) on TAS (GFn are guide fields; Nn and Pn are respectively the nutation and precession coils; M1 and M2 are two superconducting Meissner shields).

Experimental procedure

The only one existing device capable to measure accurately the transverse components of the polarization is called CRYOPAD. The principles of this device have been given in Refs. [26,27]. The principle scheme of SNP on a three-axis spectrometer is given in Figure 3.

The experimental procedure consists to determine for each incident configuration α and $\bar{\alpha}$ (α = x, y or z) the three components $P_{f\beta}(\alpha)$ (β = x, y, z) by measuring the *background-corrected* intensities $I^+_{\alpha\beta}$ and $I^-_{\alpha\beta}$ respectively associated with the $|+\rangle$ and $|-\rangle$ spin states (all together 18 contributions), according to the relation:

$$P_\beta(\alpha) = \frac{I^+_{\alpha\beta} - I^-_{\alpha\beta}}{I^+_{\alpha\beta} + I^-_{\alpha\beta}} \tag{3.40}$$

The different structure factors are deduced by taking the appropriate symmetric or antisymmetric combinations, according to the previous set of relations. Without any doubt, the major difficulty of the method in inelastic neutron scattering resides in the weakness of awaited effects, which indeed will imply rather long counting times in order to achieve the required accuracy.

4 APPLICATION OF THE NEUTRON POLARIZATION ANALYSIS

In this section, we will give characteristic examples showing the usefulness of the inelastic neutron polarimetry for the investigation of both the magnetic and structural excitations. As previously seen, the longitudinal polarization analysis is an invaluable method for the separation of various magnetic components or for the independent determination of structural and magnetic contributions. We will illustrate this fact by several examples taken in the field of low-dimensional quantum spin systems, high-T_C superconductivity, anomalous rare-earth materials, and others. The usefulness of the promising spherical neutron polarimetry will be discussed from a pioneering investigation on the spin-Peierls compound $CuGeO_3$.

4.1 Nature of non-magnetic planes in cesb

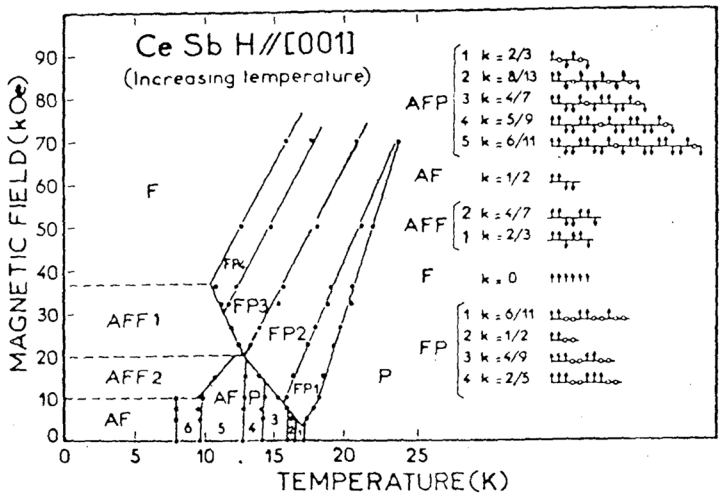

Figure 4. H-T phase diagram of CeSb.

Among the cerium compounds, the monopcitide CeSb, which crystallizes in the face-centered cubic structure, displays quite remarkable and unique magnetic properties [28]. Among others, this material is characterized by a very strong axial anisotropy of magnetic moments along the fourfold $< 001 >$ directions [29] and a very complex H-T phase diagram [30], displaying about sixteen different phases below $T_N \approx 16.5$ K. All these phases are associated with commensurate wave vectors $\mathbf{k} = [00k]$ and can be described as a stacking of (001) ferromagnetic (F) and/or non-magnetic (P) planes. For example, the AFF2 phase, which is described by the $++--++-$ sequence (associated with a wavevector component $k = 4/7$), has no non-magnetic planes, whereas the FP2 phase, which is described by the $++00$ sequence (associated with $k = 1/2$) has as many F-planes than P-planes.

A key problem to solve in CeSb concerns the understanding of the nature of these non-magnetic planes [32]. Are they paramagnetic (i.e. associated with a zero thermal average magnetization like in the paramagnetic state) or do they reflect the existence of a non-magnetic singlet ground state of Kondo-type [31]? The longitudinal polarization analysis (LPA) technique, by probing independently the SF and NSF nature of the inelastic magnetic response may bring invaluable piece of information. For a magnetic field applied along the vertical $[001]$ direction (perpendicular to the scattering $(\mathbf{a}, \mathbf{b})$), a paramagnetic crystal-field-like excitation should be both SF and NSF, with $I_{SF} \approx I_{NSF}$, whereas any singlet-triplet excitation should appears mostly SF (i.e. $I_{NSF} \approx 0$). As it is well known, for ordered magnetic moments pointing along $[001]$, the transverse spin-wave excitations associated with the F-planes should be

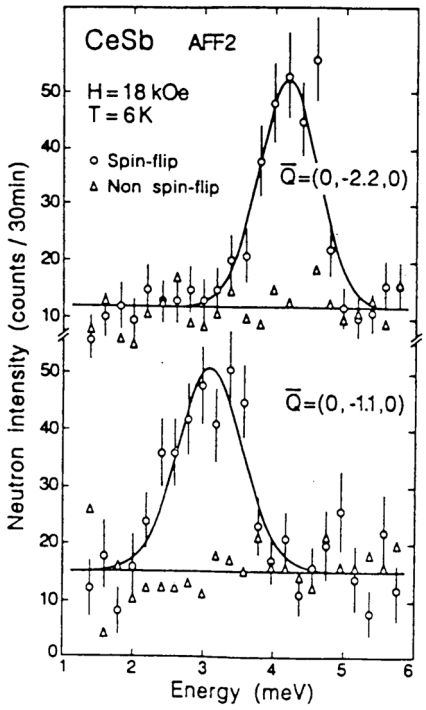

Figure 5. Zone-center and zone-boundary excitations in the AFF2 phase in CeSb.

also only SF. Polarized neutron inelastic scattering experiments have been performed in the AFF2 phase ($H = 18$ kG; $T = 6$ K), which contains no P-planes, and in the FP2 phase ($H = 18$ kG; $T = 15$ K), which contains half P-planes.

The Figure 5 displays typical constant-Q scans performed in the AFF2 phase for two scattering vectors $\mathbf{Q} = (0, -1.1, 0)$, located near the the Brillouin-zone boundary, and $\mathbf{Q} = (0, -2.2, 0)$, located near the Brillouin-zone center. As expected for purely transverse excitations, the scattered intensities appear mainly SF, whereas the mode energy (respectively 3 and 4.4 meV) follows the zero-field dispersion

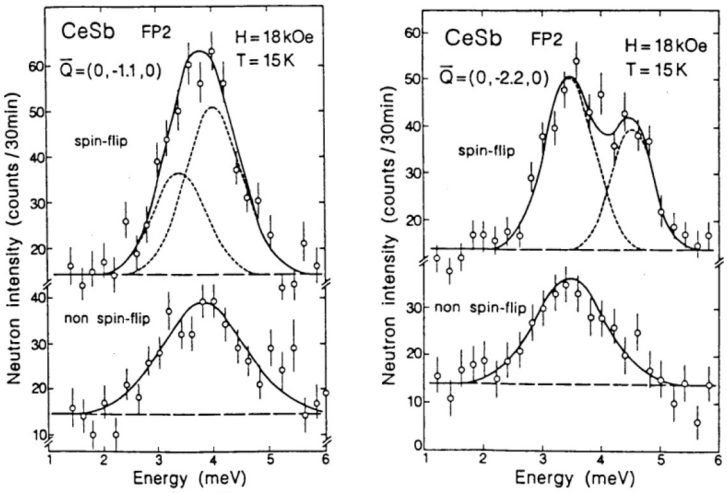

Figure 6. Zone-center and zone-boundary excitations in the FP2 phase in CeSb.

curve slightly shifted by the Zeeman energy $m_0 H \approx 0.22$ meV, corresponding to an applied field of 18 kG. Similar measurements have been performed in the FP2 phase containing as many P-planes than F-planes. The Figure 6 summarizes the main results which have been obtained. For the scattering vector $\mathbf{Q} = (0, -2.2, 0)$, associated with a wave vector located near the zone center, two distinct modes are observed in the SF channel, at energies 3.45 meV and 4.5 meV, whereas in the NSF channel only one mode is observed at about 3.45 meV. By comparison with the previous data in the AFF2 phase, the mode at 4.5 meV is attributed to the excitation in the F-planes. The mode at 3.45 meV, both SF and NSF (with $I_{SF} \approx I_{NSF}$), is attributed to the excitation in the P-planes. The results at $\mathbf{Q} = (0, -1.1, 0)$, although more difficult to analyze owing to the stronger overlap of both modes, confirm qualitatively the above conclusion. Thus, the P-planes are true *paramagnetic* planes, with a crystal-field level scheme quite similar to that observed in the paramagnetic phase above T_N. The quantitative analysis of the line shape of the inelastic response shows that the energy widths of P-modes (in particular their NSF components) are significantly larger than those of F-modes, this implying shorter life-times which are indeed well understood from the larger disorder existing in the P-planes.

4.2 Solitonic excitations in the classical antiferromagnetic chain compound TMMC

In this subsection, we will illustrate on a simple example how useful may be the longitudinal polarization analysis for the determination of the wave vector and energy dependences of various magnetic components involved in a given magnetic material. In the classical-spin Heisenberg antiferromagnetic one-dimensional (1D) system under magnetic field applied perpendicular to the chain axis, it has been established long time ago that, in addition to the usual linear *spin waves* excitations (associated with *small amplitude spin-oscillations*), non-linear excitations, the so-called *solitons*, are playing a fundamental role in the thermal behavior [33,34].

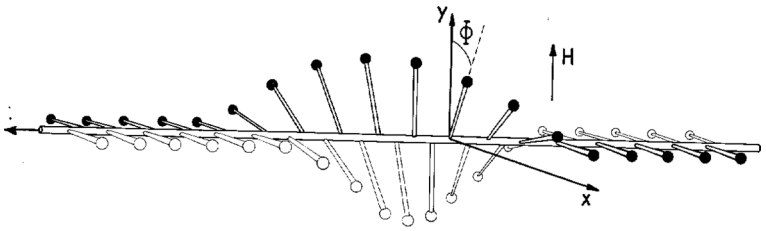

Figure 7. Antiferromagnetic-soliton structure. The soliton is nothing else than a domain wall moving along the chain axis.

These excitations, which are associated with large amplitude spin rotations (π or 2π), can be viewed as moving domain-walls, separating two different configurations of the degenerated ground state. In a quasi-1D system for which the interchain couplings can be neglected, such domain walls can move easily along the chain, giving rise to characteristic spin dynamics. In the antiferromagnetic case, the solution which minimizes the free energy corresponds to a π-rotation of each sublattice, as depicted in Figure 7. The soliton displacements induce a flipping of spins which should deeply affect the dynamical structure factors. According to the theory [33,34], the soliton energy is directly related to the field value H by the relation: $E_S = g\mu_B SH$. The average distance between two adjacent solitons defined the correlation length of the system, ξ, related to the soliton density n_S by the relation: $\xi^{-1} = 4n_S$. As it can be easily checked on Figure 7, the solitons display spin components both parallel and perpendicular to the field direction. In particular, the solitons contribute mostly to the structure factor $S_{\parallel}(q,\omega)$, while $S_{\perp}(q,\omega)$ reflects mainly the behavior of spin components between two solitons. Analytical expressions for $S_{\perp}(q,\omega)$ and $S_{\parallel}(q,\omega)$ have been derived by Mikeska [33] and Maki [34], within the framework of the non-interacting soliton-gas model.

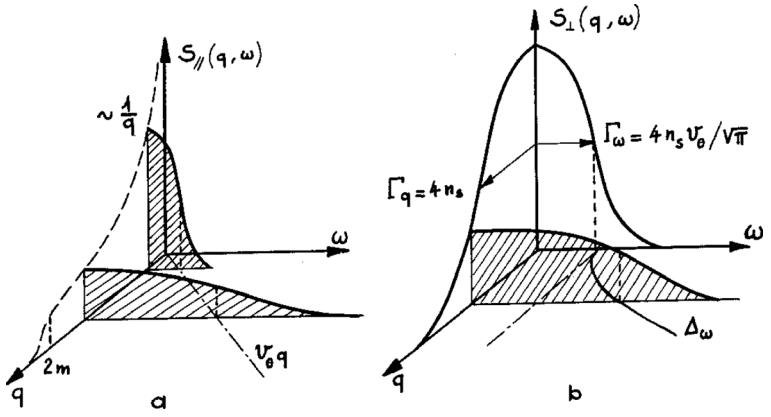

Figure 8. Theoretical structure factors $S_{\parallel}(q,\omega)$ (a) and $S_{\perp}(q,\omega)$ (b). Both give rise to quasi-elastic contributions strongly depending on T and H. The various hatched curves indicate the look of the energy dependences at various wave vectors.

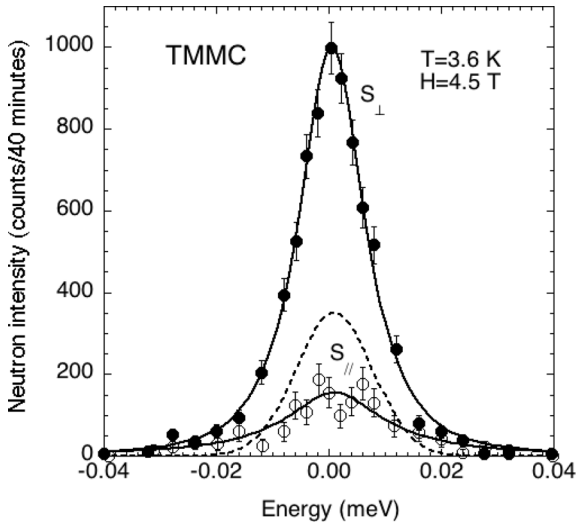

Figure 9. Frequency spectra of magnetic fluctuations observed in directions parallel and perpendicular to the external field (∘ and •, respectively).

Both contributions are of quasi-elastic type, centered around $q \approx \pi$ and $\omega \approx 0$ and given by the following relations:

$$S_{\perp}(q,\omega) \propto \frac{\Gamma_\omega/\Gamma_q}{[{\Gamma_\omega}^2 + (1+\tilde{q}^2/\Gamma_q^2) + \omega^2]^{3/2}} \tag{4.1}$$

in which the characteristic widths $\Gamma_q \approx 4n_S$ and $\Gamma_\omega \approx 4n_S v_0$, where $v_0 \approx c_0\sqrt{\frac{2k_BT}{\pi E_S}}$ is the average quadratic thermal velocity of solitons, related to the spinwave velocity $c_0 \approx 2Ja$ and the soliton energy E_S, and,

$$S_{\parallel}(q,\omega) \propto \frac{n_S\, e^{-(\omega/v_0\tilde{q})^2}}{v_0\tilde{q}\cosh^2(\pi\tilde{q}/2m)} \tag{4.2}$$

where $\tilde{q} = q - \pi$, $n_S \approx \sqrt{\frac{2}{\pi}}\frac{E_S}{JS^2}\sqrt{\frac{E_S}{k_BT}}e^{-\frac{E_S}{k_BT}}$ and $m = \frac{E_S}{2JS^2a}$ is the soliton mass. In Eqs.(4.1) and (4.2), a and J are respectively the spin-spin distance and coupling constant. The schematic dependences

on q and ω of the theoretical structure factors $S_\perp(q,\omega)$ and $S_\parallel(q,\omega)$ are given Figure 8a ($S_\parallel$) and 8b ($S_\perp$). For usual conditions of observation, $T \sim 2$ to 5 K and $H \sim 2$ to 5 T, the spatial extension of the soliton is at least one order of magnitude smaller than the average inter-soliton distance, implying that $S_\parallel(\pi,0) \ll S_\perp(\pi,0)$. Consequently, it will be quasi-impossible to determine $S_\parallel(q,\omega)$ by means of unpolarized neutron scattering [35]. Contrary, the longitudinal polarimetry with $\mathbf{P}_0 \parallel \mathbf{H}$ is particularly well suited, for the reason that $S_\parallel(q,\omega)$, associated with spin components parallel to the field, is entirely NSF, while $S_\perp(q,\omega)$, associated with spin components perpendicular to the field, is entirely SF. An example of experimental result is given in Figure 9 for a temperature $T = 3.6$ K and a field $H = 4.5$ T. The details of the experimental set-up and data analysis can be found in reference [36]. For $S_\perp$, the experimental situation can be reproduced from Eq.4.1 describing the flipping-mode within the non-interacting soliton-gas model. However, as shown by the dashed line in Figure 9, this too simplistic model is by far unable to account quantitatively for $S_\parallel$. A much better agreement (solid lines in Figure 9) can be obtained by taking into account the dynamical damping of the soliton mode (arising from the soliton-magnon and soliton-soliton interactions [37]) and additional thermal renormalization effects [36]. To our best knowledge, the LPA is the only one technique allowing to investigate directly the field and temperature dependences of soliton-like excitations.

4.3 Separation of magnetic and lattice contributions in the high-T_C superconductor $YBa_2Cu_3O_{6+x}$

A further very interesting feature of the LPA concerns its ability in separating the structural and magnetic contributions, which may appear superposed in a more or less large part of the $\mathbf{q} - \omega$ space. This is especially the case for the high-T_c superconducting cuprate $YBa_2Cu_3O_{6+x}$ (YBCO). One generic feature of the high-T_c superconductors is that they all contain CuO_2 layers, which in the undoped parent compounds form quasi-2D antiferromagnetic insulators [38,39,40,41]. This could indicate that the coupling mechanism is mediated by magnetic fluctuations, which indeed have been found to undergo profound changes as the materials are doped from antiferromagnetic insulators to superconducting metals [41,42].

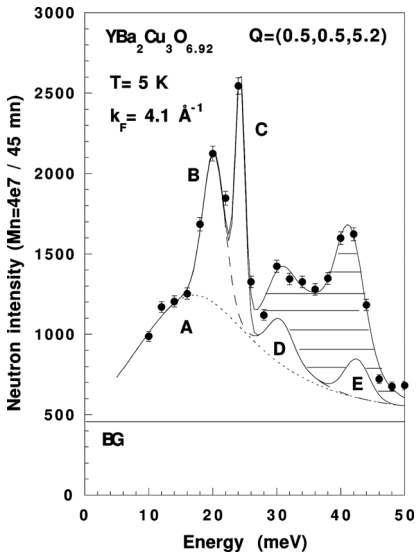

Figure 10. Typical unpolarized-neutron constant-Q scan at $\mathbf{Q} = (0.5, 0.5, 5.2)$ in the superconducting phase of $YBa_2Cu_3O_{6.92}$, showing the different contributions to the scattering (A, B, D and E: inelastic strucural contributions; C: Bragg contamination; BG: Background; Hatched area: magnetic signal).

Even if they do not appear directly responsible for the unconventional pairing mechanism, these magnetic fluctuations at least provide an important probe to the nature of the phenomenon. Therefore, one of the key points to the understanding of the pairing mechanism in high-T_C cuprates is the precise determination of the temperature- and doping-dependences of magnetic and lattice excitation spectra. In YBCO, this problem has been tackled in the early 90's, from very comprehensive unpolarized inelastic neutron scattering experiments (see, e.g. Refs. [39,41]). In most of investigations, the difficulty was to extract the relevant magnetic contributions from the nuclear ones (like, e.g., Bragg parasitic contributions, multiple-scattering, phononic contributions, etc). The problem is well illustrated at Figure 10, which depicts a typical unpolarized neutron constant-Q scan obtained in the slightly underdoped material $YBa_2Cu_3O_{6.92}$, superconducting below 92 K.

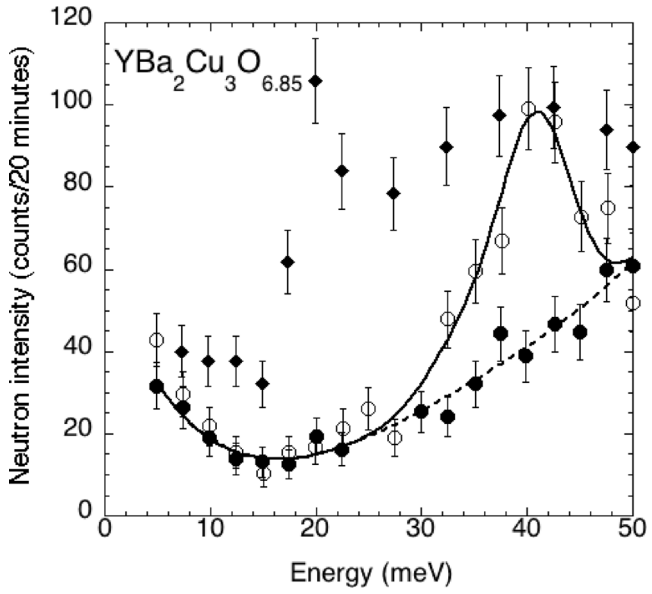

Figure 11. Sin-flip (○) and non-spin-flip (♦) constant-Q scans at the antiferromagnetic zone center at $\mathbf{Q} = (1.5, 0.5, 1.7)$ and at a background position $\mathbf{Q} = (1.8, 0.6, 1.7)$ (•), in the configuration $\mathbf{P}_0 \parallel \mathbf{Q}$ allowing a clean separation of magnetic and structural contributions.

In that case, the magnetic contribution (hatched area) could be partly estimated from a careful analysis of the temperature dependence of the inelastic scattering. The LPA method, from measurements of the SF and NSF contributions in the configuration $\mathbf{P}_0 \parallel \mathbf{Q}$, can bring a much simpler and efficient solution to the problem. As previously explained, within such a configuration the lattice excitations should only contribute to the NSF channel, whereas the magnetic ones should only contribute to the SF channel, thus allowing a quasi-perfect separation of structural and magnetic degrees of freedom. A typical result is shown at Figure 11, which displays NSF and SF constant-Q scans in $YBa_2Cu_3O_{6.85}$ ($T_C \approx$ 89 K) at the antiferromagnetic zone center $\mathbf{Q} = (1.5, 0.5, 1.7)$, these allowing to determine separately the lattice and magnetic contributions [43,44]. As it is now well admitted, the main feature of the magnetic excitation spectrum in superconducting $YBa_2Cu_3O_{6+x}$ near optimal doping (i.e. $x \approx 0.95$) is the presence of a resonant mode (vanishing at T_C), peaked at the antiferromagnetic zone center (π,π) and at the characteristic energy $E_R \approx 41$ meV. At the accuracy of the polarized neutron experiments, the magnetic spectral weight for $x \approx 0.85$ is non-vanishing only in the range $25 - 50$ meV (corresponding to the hatched area in Figure 11). Interestingly, the resonant peak is a magnetic feature of the superconducting state, centered around (π, π) and vanishing almost completely in the normal state [41].

4.4 Magnetic excitation spectrum of the S=1/2 spin-Peierls compound $CuGeO_3$

The germanate $CuGeO_3$ is considered in the literature as a good prototype of the spin-Peierls system [45,46,47,49]. Below a characteristic temperature $T_{SP}\approx$ 14 K, the so-called spin-Peierls transition temperature, the magnetic susceptibilities along the three main crystallographic directions drop exponentially to zero [45], whereas simultaneously a distortion (indeed a dimerization described by the structural wave vector k_{SP}=$(1/2, 0, 1/2)$) develops at low temperature [48].

In this material strong spin-lattice couplings are present, which are responsible for the dimerization, the non-magnetic singlet ground state and the opening of a gap $\Delta_{sp} \approx 1.76kT_{SP}$ in the magnetic excitation spectrum. Interestingly, the spin-lattice interactions might also generate hybrid (coupling the lattice and magnetic degrees of freedom) which could give rise to non-vanishing INMI terms. The magnetic excitation spectrum of $CuGeO_3$ has been exhaustively studied by means of unpolarized neutron inelastic scattering [46,47]. According to the neutron data, the gap energy (indeed the energy corresponding to the maximum of the magnetic response at $q = \pi$) amounts to $\Delta_{SP} \approx 2$ meV at the *antiferromagnetic* (AF) scattering vectors $Q = (0, Q_k, Q_l)$ with $Q_k = 2k + 1$ and $Q_l = l + 1/2$ (k and l integer).

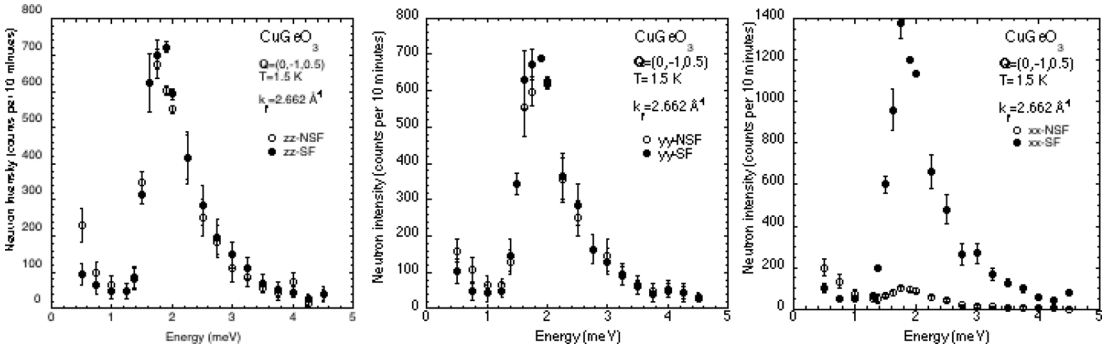

Figure 12. Constant-Q san at $\mathbf{Q} = (0, -1, 1/2)$ showing the NSF and SF contributions in three configurations $\mathbf{P}_0 \parallel$ and $\perp \mathbf{Q}$.

As seen from comprehensive unpolarized neutron inelastic scattering measurements, the spin-Peierls mode displays a strong dispersion along the b-direction (perpendicular to the chain axis), with a zone-boundary energy $\hbar\omega(q_b = 1) \approx 5.6$ meV [46,47]. Full LPA measurements have been performed on $CuGeO_3$, in order to determine separately the various magnetic and structural components involved in the spin-Peierls mode [43,44]. In Figure 12 is depicted the same constant-Q scan performed at the scattering vector $\mathbf{Q} = (0, -1, 1/2)$, which shows the SF and NSF contributions associated with the 2-meV spin-Peierls mode for an initial polarization $\mathbf{P}_0$ successively directed along **x** (P_{xx}), **y** (P_{yy}) and **z** (P_{zz}). As expected for any mainly magnetic mode, the 2-meV mode appears almost completely SF for $\mathbf{P}_0 \parallel \mathbf{Q}$ ($P_{xx} \approx -P_0$) and almost entirely depolarized for $\mathbf{P}_0 \perp \mathbf{Q}$ ($P_{yy} \approx P_{zz} \approx 0$), the latter results showing, among others, the weak anisotropy of the spin-spin correlation functions, which contrast with the strong anisotropy of the g-tensor seen in the susceptibility measurements. Neglecting the NMI and chiral terms, one can make use of Eq.(3.16) which relates the nuclear contribution to the three longitudinal polarizations P_{xx}, P_{yy} and P_{zz} in order to determine the underlying nuclear contribution. In $CuGeO_3$, one obtains the longitudinal components as $P_{xx} \approx -0.870(5)$, $P_{yy} \approx 0.000(5)$ and $P_{zz} \approx -0.030(5)$ [62], implying a ratio $\frac{N}{M_{yy}+M_{zz}} \approx 0.001 \pm 0.002$ which confirms quantitatively the mainly magnetic nature of the spin-Peierls mode at 2 meV. This result is in agreement with the standard spin-Peierls theory in the weak-coupling limit [52].

4.5 Chiral contributions in $Sr_{14}Cu_{24}O_{41}$ under applied magnetic field

In this section, we will illustrate the power of the longitudinal polarization analysis for the characterization and the understanding of the nature of magnetic excitations in strongly correlated electron systems. The cuprate $Sr_{14}Cu_{24}O_{41}$ is a very fascinating material, the crystallographic structure of which can be described as a misfit stacking of layers of two distinct $S = 1/2$ spin systems: linear CuO_2 chains and 2-leg Cu_2O_3 spin-ladders [53]. This compound naturally contains a large amount of hole carriers (0.6 holes/Cu), mainly localized in the chains [54,55,56]. By substitution of Ca^{2+} for Sr^{2+}, holes are transferred from the chains to the ladders [55,56] and the compound undergoes an insulator-metal transition at ambiant pressure [54,55,56,57] and superconductivity is observed above 3 Gpa [58].

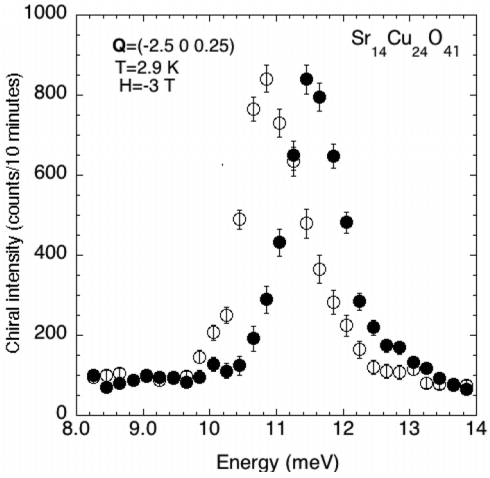

Figure 13. Polarization analysis of the inelastic scattering of an unpolarized neutron beam on the gapped mode at $\mathbf{Q} = (-2.5, 0, 0.25)$ in the CuO_2 chains of $Sr_{14}Cu_{24}O_{41}$ under an applied magnetic field of 3 T. Open and closed symbols represents respectively the $|-\rangle$ and $|+\rangle$ final neutron-spin states.

The magnetic excitation spectra in both the chains [60] and ladders [23,59] have been investigated from comprehensive inelastic-neutron-scattering measurements. Quite interestingly, gaps associated with singlet-triplet excited modes have been observed in the range 10–12 meV for the chains [60] and around 32–33 meV for the ladders [59]. In agreement with the susceptibility and transport measurements [54], the in-chain gap has been attributed to the existence of weakly correlated $\uparrow\ 0\ \downarrow$ spin-1/2 dimers, whereas the holes appeared long-range ordered at low temperature (defining a hole crystal). As previously explained, the inelastic chiral contribution can be determined from the measurement of the polarization after scattering, starting from a non-polarized beam and applying the magnetic field along the scattering vector. Within such a configuration, the triplet gap at $q = \pi$ should split linearly under field into two modes with energies $\Delta_0 \pm g\mu_B H$, while the third mode (constant in energy and associated with spin-components parallel to the field and $\mathbf{Q}$) should not contribute to the magnetic scattering. The Figure 13 summarizes the polarization analysis of the inelastic scattering at $\mathbf{Q} = (-2.5, 0, 0.25)$, under an applied magnetic field of 3 T [61].

Among others, these results confirm the shift by $\pm g\mu_B H \approx \pm 0.3$ meV of the in-chain gap around 11.2 meV. They also demonstrate the fully-SF nature of the scattering. Interestingly, the scattered neutron beam appears fully polarized, a fact implying necessarily the existence of a rather-strong chiral term and time-reversal-symmetry breaking [61]. The dependence on energy of the chiral contribution, obtained from the difference $I_+ - I_-$, is displayed in Figure 14. In agreement with the discussion in section 3.2, the chiral contribution is an odd function of the energy centered around the energy-gap value. According to the general expressions (3.1) and (3.2), such a strong chiral term should reflect the

existence of large *transverse* spin-spin correlation functions, coupling spin components along the $\mathbf{y}$ and $\mathbf{z}$ directions, with qualitatively $\langle S_y S_z \rangle \sim \langle S_y S_y \rangle \sim \langle S_z S_z \rangle$. Such a behavior may be easily understood within the general picture following which the excited states correspond to a field-induced collective precession of spins, turning clockwise or counterclockwise around the field direction, with the Larmor pulsation $\pm g\mu_B H/\hbar$. This example illustrates very well the time-reversal-breaking-down mechanism induced by an applied magnetic field.

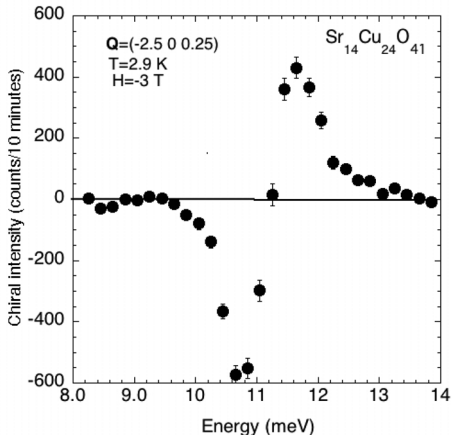

Figure 14. Energy dependence of the difference of intensities associated with the $|+\rangle$ and $|-\rangle$ neutron spin states at $\mathbf{Q} = (-2.5, 0, 0.25)$, showing the strong chiral contribution in $Sr_{14}Cu_{24}O_{41}$.

4.6 Spherical polarimetry on $CuGeO_3$

In this section we will show how the SNP may help to solve the full problem, namely the determination of the complete set of correlation functions involving the nuclear and magnetic degrees of freedom. The spin-Peierls compound $CuGeO_3$ appeared to be a very suitable candidate to perform such a determination, owing to the strong spin-lattice interactions existing in this material. In section 4.5, it was shown that the nuclear structure factor associated with the hypothetic *hybrid* mode was very small, amounting to at best 0.3% of the main magnetic structure factor at $q = \pi$. However, if the hybrid correlation function between the magnetic and structural degrees of freedom was strong-enough, it might give rise to a sizable NMI term and, thus, a small rotation of the polarization away from $\mathbf{P_0}$ should be detected. Maleyev [9] and Cepas et *al.* [64] have considered theoretically a S=1/2 spin-Peierls system described by *dynamical* Heisenberg (H) and Dzyaloshinski-Moriya (DM) interactions, both given by the generic term: $\sum_{i,j} \sum_{\alpha,\beta} V^{\alpha\beta}(\mathbf{R}_j - \mathbf{R}_i) S_i^\alpha S_j^\beta$, where $V^{\alpha\beta}(\mathbf{R}_j - \mathbf{R}_i) = J_\beta(\mathbf{R}_j - \mathbf{R}_i)\delta_{\alpha\beta}$ for the former and $\sum_\gamma D_\gamma(\mathbf{R}_j - \mathbf{R}_i)\epsilon_{\gamma\alpha\beta}$ for the latter, where the D_γ coefficients are the components of the Dzyaloshinski-Moriya vector, which depend on the position of all ions involved in the superexchange paths. Maleyev [9,10,11], by using the standard perturbation theory, has found that the INMI terms are related to the three-spin suceptibilities (or, equivalently, to the three-spin correlation functions), following the expression:

$$\langle N_Q^+ \mathbf{M}_Q \rangle_\omega = N^{\frac{-1}{2}} \sum_{n,i,j} b_n \sum_{\alpha,\beta} \langle e^{-i\mathbf{Q}\cdot\mathbf{R}_n}, V_{ij}^{\alpha\beta} \rangle_\omega \langle S_i^\alpha S_j^\beta, \mathbf{M}_Q \rangle_\omega \tag{4.3}$$

In Eq.(4.3), the magnitude of NMI terms appears controlled by the first angle-bracket, which may be non-zero if the lattice excitations modulate both $\mathbf{R}_n$ and the V components. For a system presenting no long-range order, as it is the case for $CuGeO_3$, the scalar Heisenberg-exchange terms give no contribution to the NMI and only the Dzyloshinski-Moriya term can contribute. According to the general

theory [10,11,64], the expression giving the INMI terms contain factors $\frac{1}{\omega^2-\omega_\lambda^2}$, where ω_λ is the phonon energy and λ labels the different phonon (acoustic or optic) branches. Thus, the INMI terms must be a priori searched near scattering vectors for which the magnetic and nuclear contributions are not too far in energy. Obviously, the amplitude of INMI terms should also depend drastically on the polarization of the phonon involved in the interference process (remember that in a inelastic-neutron-scattering experiment one cannot measure simultaneously the spin components and the atomic displacements along the same direction). In order to verify these predictions, a spherical polarization analysis of the 2-meV mode on $CuGeO_3$ must be performed by using the CRYOPAD device. As previously explained, the procedure consists to determine, for each couple $(\mathbf{Q},\omega)$, the 18 components $P_{\alpha\beta}$ and $P_{\bar{\alpha}\beta}$ $(\alpha,\beta=x,y,z)$ of the polarization matrix, after the appropriate background corrections. Table 2 gives the values of $P_{\alpha\beta}$ and $P_{\bar{\alpha}\beta}$ $(\alpha,\beta=x,y,z)$ and the corresponding error bars for the spin-Peierls mode at $\mathbf{Q}=(0,1,1/2)$ [62,63].

Table 2. Spherical polarization analysis of the 2-meV mode at $\mathbf{Q}=(0,1,1/2)$ in $CuGeO_3$. Longitudinal and transverse components of the polarization matrix.

$\alpha\beta$	$P_{\alpha\beta}(\pm\Delta P)$	$\bar{\alpha}\beta$	$P_{\bar{\alpha}\beta}(\pm\Delta P)$
xx	–0.868 (6)	$\bar{x}x$	0.866 (6)
xy	–0.034 (8)	$\bar{x}y$	0.044 (8)
xz	–0.015 (8)	$\bar{x}z$	0.025 (8)
yx	0.004 (8)	$\bar{y}x$	0.021 (8)
yy	0.001 (8)	$\bar{y}y$	–0.008 (8)
yz	0.006 (8)	$\bar{y}z$	0.001 (8)
zx	0.006 (8)	$\bar{z}x$	0.015 (8)
zy	–0.004 (8)	$\bar{z}y$	–0.004 (8)
zz	–0.031 (8)	$\bar{z}z$	0.026 (8)

From Table 2, one can deduce the longitudinal components:

$$\overline{P}_{xx}=(-0.963\pm0.005)P_0$$
$$\overline{P}_{yy}=(0.005\pm0.006)P_0$$
$$\overline{P}_{zz}=(-0.031\pm0.006)P_0$$

with $P_0=0.89\pm0.005$, and where $\overline{P}_{\alpha\alpha}=\frac{P_{\alpha\alpha}-P_{\bar{\alpha}\alpha}}{2}$ is the antisymmetric part which cancels at first order the P_0-independent terms. Undouptly, CRYOPAD allows a very precise determination of the longitudinal components, the limitation being mainly due to the statistical error on the counting (the intrinsic error is smaller than 0.0005!). In agreement with the LPA measurements, the quantity $\frac{\overline{P}_{xx}+\overline{P}_{yy}+\overline{P}_{zz}}{P}_0=(-0.989\pm0.010)$ is very close to 1, which again means that the nuclear contribution associated with the putative hybrid mode at $q=\pi$ should be very small: $\frac{N}{\sigma_0}=(0.003\pm0.003)$, as previously found from LPA.

Applying the set of relations given in section 3.2, it has been possible to get relatively reliable estimates of the magnetic and INMI terms:

$$M_{yy}-M_{zz}=0.015\pm0.010$$
$$M_{ch}/\sigma_0=0\pm0.003$$
$$M_{yz}/\sigma_0=-0.003\pm0.003$$
$$R_y/\sigma_0=0\pm0.004$$
$$I_y/\sigma_0=-0.008\pm0.005$$

$$R_z/\sigma_0 = 0.004 \pm 0.004$$
$$I_z/\sigma_0 = -0.015 \pm 0.005$$

Thus, within the error bars, the chiral term and the symmetric INMI terms appear to be very small, while the antisymmetric INMI terms (especially I_z) appear finite, although at the limit of the accuracy of the present CRYOPAD version (roughly ± 0.01). To summarize the results of the SNP on the spin-Peierls mode in $CuGeO_3$, the magnitude of INMI terms is found to be at best 1% of the main magnetic signal. At $q \approx \pi$ and $\hbar\omega \approx \Delta_{SP}$, the magnetic and lattice excitations can be considered as almost completely decoupled. The main reason for this negative result comes from the fact that in $CuGeO_3$ $\Delta_{SP} \ll \omega_{ph}$. Hybrid modes may exist at other q or energy values, in particular those corresponding to the continuum [65]. Unfortunately, despite several tentatives, they have not been detected so far.

5 CONCLUSION

In this chapter, we have shown how powerful is the neutron polarimetry for the investigation of inelastic spectra in condensed-matter physics. The most-frequently-used method, namely the longitudinal polarization analysis (alias LPA), is best suited for all studies requiring the accurate determination of dynamical spin-spin correlation functions involving only the longitudinal components of the generalized-susceptibility tensor. Among others things, the LPA allows to obtain separately the structural and various longitudinal magnetic structure factors (e.g, the P_0-dependent parts, chiral terms, anisotropy of various spin-spin correlation functions). Basically, the LPA can be used to solve problems for which the nuclear-magnetic interference terms can be neglected. If strong enough, such terms might produce a rotation of the polarization vector around the interaction vector different from π, which can be only determined by spherical neutron polarimetry (alias SNP). In principle, the measurement of the nine coefficients of the polarization matrix should allow to unambiguously solve the full problem and, finally, should allow to determine the various nuclear-nuclear, magnetic-magnetic and nuclear-magnetic correlation functions. Unfortunately, no transverse components of the polarization could be detected so far, just by lack of good experimental system.

References

[1] Halpern, O., and Johnson, M.H., *Phys. Rev.* **55**, 898 (1939).
[2] Halpern, O., and Holstein, T., *Phys. Rev.* **59**, 960 (1941).
[3] Maleyev, S.V., *Sov. Phys. JETP* **13**, 595 (1961).
[4] Izyumov, Yu., and Maleyev, S.V., *Sov. Phys. JETP* **14**, 1168 (1962).
[5] Izyumov, Yu., *Sov. Phys. JETP* **15**, 1167 (1962).
[6] Maleyev, S.V., Baryakhtar, V.G., and Suris, A., *Sov. Phys. Solid State* **4**, 2533 (1963).
[7] Blume, M., *Phys. Rev*. **130**, 1670 (1963). and references therein.
[8] Schermer, R.I., and Blume, M., *Phys. Rev*. **166**, 554 (1968).
[9] Maleyev, S.V., *Physica B* **267–268**, 236 (1999).
[10] Maleyev, S.V., *Physica B* **297**, 67 (2001)
[11] Maleyev, S.V., *Physics-Uspekhi* **45**, 569 (2002). and references therein
[12] Trammell, G.T., *Phys. Rev*. **92**, 1387 (1953).
[13] Lovesey, S.W., in *Theory of Neutron Scattering from Condensed Matter*, vol. 1 and 2, Clarendon Press, Oxford, 1987.
[14] Balcar, E., and Lovesey, S.W., in *Theory of Magnetic Neutron and Photon Scattering*, Clarendon Press, Oxford, 1989.

[15] Van Hove, L., *Phys. Rev.* **95**, 249 (1954).
[16] Schwinger, J., *Phys. Rev.* **73**, 407 (1948).
[17] Blume, M., *Phys. Rev.* **133**, A1366 (1964).
[18] Squires, G. L., in *Introduction to the theory of thermal neutron scattering*, Dover publications, Mineola, New York, 1986.
[19] Moon, R.M., Riste, T., and Koehler, W.C., *Phys. Rev.* **181**,920 (1969).
[20] Drabkin, G.M., *et al*., *JETP Lett.* **2**, 353 (1965).
[21] Brehmer, S., *et al*., *Phys. Rev. B* **60**, 329 (1999).
[22] Muller, M., *et al*., *Phys. Rev. B* **66**, 34423 (2002).
[23] Matsuda, M., *et al*., *Phys. Rev. B* **62**, 8903 (2000).
[24] Maleyev, S.V., *Phys. Rev. Lett.* **75**, 4682 (1995) and references therein.
[25] Aristov, D.N., and Maleyev, S.V., *Phys. Rev. B* **62**, R751 (2000) and references therein.
[26] Tasset, F., *Physica B* **156–157**, 627 (1989).
[27] Brown, P.J., Forsyth, J.B., and Tasset, F., Proc. R. Soc. London A **442**, 147 (1993).
[28] Rossat-Mignod, J., Burlet, P., Quezel, S., and Vogt, O., *Physica B* **102**, 237 (1980).
[29] Bartholin, H., Florence, D., Wang Tcheng-Si, and Vogt, O., *Phys. Status Solidi A* **24**, 631 (1974).
[30] Rossat-Mignod, J., Burlet, P., Villain, J., Bartholin, H., Wang Tcheng-Si, Florence, D., and Vogt, O., *Phys. Rev. B* **16**, 440 (1977).
[31] Takahashi, H., and Kasuya, T., *J. Phys. C* **18**, 2697 (1985).
[32] Regnault, L.P., Jacoud, J.L., Vettier, C., Chattopadhyay, T., Rossat-Mignod, J., Suzuki, T., Kasuya, T., and Vogt, O., *Physica B* **156 & 157**, 798 (1989).
[33] Mikeska, H., *J. Phys. C* **13**, 2913 (1980).
[34] Maki, K., *J. Low. Temp. Phys.* **41**, 327 (1981).
[35] Regnault, L.P., Boucher, J.P., Rossat-Mignod, J., Renard, J.P., Bouillot, J., and Stirling, W.G., *J. Phys. C* **15**,1261 (1982) and references therein.
[36] Boucher, J.P., Regnault, L.P., Pynn, R., Bouillot, J., and Renard, J.P., *Europhys. Lett.* **1**, 415 (1986) and references therein.
[37] Sasaki, K., in Proceedings of the VII Kyoto Summer Institute, edited by S. Takeno (Springer, Berlin, 1985).
[38] Vaknin, D., *et al.*, *Phys. Rev. Lett*. **58**, 2802 (1987).
[39] Rossat-Mignod, J., *et al.*, *Physica C* **185–189**, 86 (1991).
[40] Fong, H.F., *et al.*, *Phys. Rev. Lett.* **75,** 316 (1995); H. F. Fong *et al.*, Nature **398**, 588 (1999).
[41] Regnault, L.P., Bourges, P., and Burlet, P., in *Neutron Scattering in Layered Copper-oxyde Superconductors*, edited by A. Furrer (Kluwer Academic Publishers, DORDRECHT/BOSTON/ LONDON, 1998) p. 85–134 and references therein.
[42] Hayden, S., in *Neutron Scattering in Layered Copper-oxyde Superconductors*, edited by A. Furrer (Kluwer Academic Publishers, DORDRECHT/BOSTON/LONDON, 1998) p. 135–164 and references therein.
[43] Regnault, L.P., *et al.*, *Physica B* **335**, 19-25 (2003).
[44] Regnault, L.P., *et al.*, *Physica B* **345**, 111–118 (2004).
[45] Hase, M., Terasaki, I., and Uchinokura, K., *Phys. Rev. Lett.* **70**, 3651 (1993).
[46] Nishi, M., Fujita, O., and Akimitsu, J., *Phys. Rev. B* **50**, 6508 (1994).
[47] Regnault, L.P., AŢn, M., Hennion, B., Dhalenne, G., and Revcolevschi, A., *Phys. Rev. B* **53**, 5579 (1996) and references therein.
[48] Pouget, J.P., Regnault, L.P., Aïn, M., Hennion, B., Renard, J.P., Veillet, P., Dhalenne, G., and Revcolevschi, A., *Phys. Rev. Lett*. **72**, 4037 (1994). *Phys. Rev. Lett*. **78**, 1560 (1997).

[49] Boucher, J.P., and Regnault, L.P., *J. Phys. I, France*, **6**, 1939 (1996) and references therein.

[50] Lorenzo, J.E., Regnault, L.P., Hennion, B., Aïn, A., Bourdarot, F., Kulda, J., Dhalenne, G., and Revcolevschi, A., *J. Phys. : Condensed Matter* **9**, L211 (1997).

[51] Bouzerar, G., Legeza, O., and Ziman, T., *Phys. Rev. B* **60**, 15278 (1999).

[52] Pytte, E., Phys. Rev. B **10**, 4637 (1974); Cross, M.C., and Fischer, D.S., *Phys. Rev. B* **19**, 402 (1979); Bray, J.W., Interrante, L.V., Jacobs, I.S., and Bonner, J.C., in *Extended Linear Chain Compounds*, edited by Miller, J.S., (Plenum, New York, 1982), Vol. 3, pp. 353–415.

[53] McCaron, E.M., Subramaniam, M.A., Calabrese, J.C., and Harlow, R.L., Mater. Res. Bull. **23**, 1355 (1988).

[54] Kato, M., Shiota, K., and Koike, Y., *Physica C* **258**, 284 (1996).

[55] Mizuno, Y., Tohyama, T., and Maekawa, S., *J. Phys. Soc. Jpn* **66**, 937 (1997).

[56] Osafune, T., Motoyama, N., Eisaki, H., and Uchida, S., *Phys. Rev. Lett.* **78**, 1980 (1997).

[57] Motoyama, N., Osafune, T., Kakeshita, T., Eisaki, H., and Uchida, S., *Phys. Rev. B* **55**, 3386 (1997).

[58] Uehara, M., Nagata, T., Akimitsu, J., Takahashi, H., Môri, N., and Kinoshita, K., *J. Phys. Soc. Jpn.* **65**, 2764 (1997).

[59] Matsuda, M., and Katsumata. K., *Phys. Rev. B* **53**, 12201 (1996).

[60] Regnault, L.P., Boucher, J.P., Moudden, H., Lorenzo, J.E., Hiess, A., Ammerahl, U., Dhalenne, G., and Revcoloevschi, A., *Phys. Rev. B* **59**, 1055 (1999).

[61] Boullier, C., Regnault, L.P., Lorenzo, J.E., Dhalenne, G., and Revcoloevschi, A., to be published.

[62] Regnault, L.P., Ronnow, H.M., Lorenzo, J.E., Bellissent, R., and Tasset, F., *Physica B* **335**, 19–25 (2003).

[63] Regnault, L.P., Ronnow, H.M., Boullier, C., Lorenzo, J.E., and Marin, C., *Physica B* **345**, 111–118 (2004).

[64] Cepas, O., and Ziman, T., in: *Quantum properties of low-dimensional antiferromagnets*, eds. Ajiro, Y. and Boucher, J.P., (Kyushu University Press, 2002), pp.175–182.

[65] Braden, M., Hennion, B., Pfeuty, P., Dhalenne, G., and Revcolevschi, A., *Phys. Rev. Lett.* **83**, 1858 (1999).